High Temperature Limit Analysis of Pressure Vessels and Piping with Local Wall-Thinning

X. Du, Y. Liu and J. Zhang

Abstract In order to evaluate the safety and integrity of pressure vessels containing volume defects and piping with local wall-thinning at elevated temperature, a numerical method for plastic limit load of modified 9Cr-1Mo steel pressure vessel and piping is proposed in the present paper. The limit load of pressure vessel and piping at high temperature is defined as the load-carrying capacity after the structure has served for a certain time period. The power law creep behavior with Liu-Murakami damage model is implemented into the commercial software ABAQUS via CREEP for simulation, and the Ramberg-Osgood model is modified to consider the material deterioration effect of modified 9Cr-1Mo steel by introducing the creep damage factor into the elasto-plastic constitutive equation. For covering the wide ranges of defect ratios and service time periods, various 3-D numerical examples for the pressure vessels with different sizes of volume defects, the piping with local wall-thinning defects, and creep time are calculated and analyzed. The limit loads of the defected structures under high temperature are obtained through classic zero curvature criterion with the modified Ramberg-Osgood model, and the typical failure modes of these pressure vessels and piping are also discussed. The results show that the plastic limit load of pressure vessel and piping containing defect at elevated temperature depends not only on the size of defect, but also on the creep time, which is different from the traditional plastic limit analysis at room temperature without material deterioration.

X. Du · Y. Liu (✉)
Department of Engineering Mechanics, Tsinghua University, Beijing 100084, China
e-mail: yhliu@mail.tsinghua.edu.cn

J. Zhang
Sino-French Institute of Nuclear Engineering and Technology,
Sun Yat-sen University, Zhuhai, China

O. Barrera et al. (eds.), *Advances in Direct Methods for Materials and Structures*, DOI 10.1007/978-3-319-59810-9_12

1 Introduction

With the rapid development of modern industry, it is estimated that the world demand for power supplies will increase by up to 50% in the next two decades [1]. Actually, it's inevitable for the appearance of defects with various dimensions for the pressure vessels and piping which are operated at elevated temperature. The defects of local wall-thinning can reduce the load-carrying capacity of pressure vessels and piping, even can lead to the leaking and explosion accident. Thus, the safety and integrity assessment of the pressure vessels and piping which should be serviced at elevated temperature for a long time becomes more significant.

The limit analysis is a method which is widely used for the pressure vessels with volume defect and the piping with local wall-thinning defect in the structure safety and integrity assessment at room temperature. The limit load of structure can be obtained by limit analyses, which is a theoretical foundation for rational design and safety assessment of pressure vessel and piping. In 1950s, the complete theory of upper and lower bound for limit analysis was presented by Drucker and Hill [2, 3]. Then, the plastic limit analysis for axial symmetry shell and plate structures was studied by Hodge and Belytschko [4–6]. Maier and Munro [7] reviewed the engineering application of plastic limit analysis. It can be found that the researches on the above are based on simple structures such as beam, axial symmetry shell and plane problems. However, it's difficult to obtain the analytical limit load solution for the complex structures in engineering. With the development of finite element method (FEM) and computer hardware, numerical method are widely used for the limit analysis of complex structures. Chen [8] proposed a numerical method for limit analysis of piping with local wall-thinning under multi-loading. Han et al. [9] studied the limit moment of local wall thinning in piping under bending using FEM. Kim et al. [10] calculated the collapse moment of pipe elbows with local wall thinning using the "twice the elastic slope" (TES) method. At the same year, by using the geometrically linear FE limit analyses, Kim et al. [11] proposed the effects of local wall thinning on plastic limit loads of elbows. Mackenzie et al. [12] proposed a simple method, named the elastic compensation method which is convenience for engineering application. By using the penalty-duality algorithm and direct iteration method, Liu et al. [13–17] calculated the limit load of 3-D structure with volume defect and local wall-thinning, which is indicated that the numerical method for limit analysis of complex structures is feasible and reasonable.

These researches of the limit analysis were conducted under room temperature situation. However, it's very different for the limit load analysis of pressure vessels and piping from room temperature to elevated temperature. On one hand, the creep regime of material must be considered when the components are subjected to elevated temperature compared with the room temperature. On the other hand, the material property is considered as virgin state without damage and deterioration during the operating service at room temperature. However, the creep damage due to the material property deterioration is inevitable, which leads to the cavity growth and nucleation in the microscale and the effective load-carrying area decreasing in the macroscale. Both

of the yield strength (YS) and the ultimate tensile strength (UTS) will be reduced when creep damage mechanism is considered [18]. Consequently, the limit load will correspondingly decrease when the components have served at elevated temperature for a long time. These two aspects are vital important to expand the method of limit load analysis for structures to elevated temperature field.

The material of interest in this study is modified 9Cr-1Mo steel, which is high-chromium ferritic steels containing 9–12% chromium and has higher creep strength and corrosion resistance than the traditional chromium-molybdenum steel used in pressure vessels and piping system. The creep behavior and creep damage model of modified 9Cr-1Mo steel have been studied by several researchers during the past decades. From the microcosmic point of view, Arzt and Wilkinson [19] proposed a dislocation based model for creep, which is valid for the local and general climb of dislocations regardless of the climb mechanisms. Fournier et al. [20] introduced a micromechanically based model for predicting the cyclic softening in the 9–12%Cr martensitic steels. For modeling the creep behavior of modified 9Cr-1Mo steel, Böck and Kager [21] performed an extensive research using the finite element method. Instead of using standard evolution law for predicting long term creep, the models based on microstructural variables are proposed. In order to take the dislocation density and subgrain coarsening into account, Sklenicka et al. [22] suggested that the role of the dislocation substructure is dominant for the creep behavior of 9Cr-1Mo steel. Based on phenomenological approach, numerous creep model have been presented by researchers, such as Graham [23], McVetty [24], Conway [25] and Norton [26], and corresponding creep constitutive functions include power law, logarithmic, exponential and hyperbolic sine law have been used for representing the creep behavior respectively. Nevertheless, these models cannot be used to describe the tertiary stage of creep. To characterize the full creep curve, the continuum damage mechanics (CDM) models coupling creep, plasticity and viscoplasticity have been developed to simulate material deterioration. The creep damage model in the pioneering work is Kachanov [27] and Rabotnov [28] (K-R) model which has been widely accepted and used for predicting the tertiary creep behavior [29]. Based on the concept of K-R model, dozens of creep damage models were presented according to the various definition of damage hereafter. Chaboche et al. [30], Lemaitre et al. [31], Hayhurst et al. [32, 33], Murakami et al. [34, 35], and Dyson et al. [36] presented creep models with different number of damage factors include single, double, triple or even quadruple variables, respectively. Hyde [37] et al. used different CDM models to approach the creep damage behavior of modified 9Cr-1Mo steel and to analyze simple pressurized pipe structures conjunction with the finite element method. Based on a micromechanical consideration of void growth and coalescence under creep damage conditions, a strain controlled creep damage model was presented by Cocks and Ashby [38]. Basirat et al. [39] proposed a CDM model based on dislocation and considered precipitate to simulate the creep behavior of modified 9Cr-1Mo steel.

It is worth noting that almost all the researches on creep damage models focused on the material deterioration in creep mechanism, but the material deterioration in plastic mechanism caused by creep damage, which is the key point to the limit load analysis, has not attracted sufficient attention. Researches showed that high creep

damage accumulation rate caused by high stress level and long time, which indicates that the material deterioration for plastic regime under creep condition is dependent on stress level, creep time and evaluated temperature. Xue et al. [40] and Wang et al. [41] presented creep damage model considering material deterioration in plastic mechanism for P91 and 2.25Cr-1Mo steels respectively. However, different stress levels in structures with defects have not been considered, which is a crucial factor to the limit load analysis at elevated temperature.

In the present paper, the limit load at elevated temperature is defined as the load-carrying capacity after the structure served for a certain period of time, and the limit analysis of pressure vessels and piping with local wall-thinning at 650 °C is numerically studied. The material is modified 9Cr-1Mo steel. The Liu-Murakami creep damage model and the modified Ramberg-Osgood model are implemented simultaneously in ABAQUS via CREEP and USDFLD subroutines. The creep damage due to the material deterioration at different stress levels is also considered. In addition, a series of numerical examples are completed to investigate the effects of defect dimensions on the limit load and the failure mode of pressure vessels and piping.

2 Continuum Damage Constitutive Equations

2.1 Creep Damage Constitutive Model

At high temperature, the creep deformation is dominated and the redistribution of stress is found to be dependent on the creep constitutive laws obeyed by the material [42]. Typical creep deformation includes three regimes: primary, secondary, and tertiary creep regimes. The continuum damage mechanics (CDM) models are adopted here to characterize the full creep curve. One of the most widely used CDM model is Kachanov [27] and Rabotnov [28] (K-R) model which has a single-state damage variable. However, the creep strain rate will approach infinity when the damage parameter approach to value 1.0. Though this effect can be reduced by setting the damage parameter to 0.99 when the material fails to complete the numerical calculation, the effect of damage localization of K-R constitutive equation cannot be avoid.

Attempting to address the issue of high damage rates as the damage parameter approaches value 1.0, Liu-Murakami (L-M) model has been presented in [34]. Multiaxial forms of the L-M model are given by

$$\dot{\varepsilon}_{ij}^{c} = \frac{3}{2} A \sigma_{eq}^{n-1} S_{ij} \exp\left[\frac{2(n+1)}{\pi\sqrt{1+3/n}} \left(\frac{\sigma_1}{\sigma_{eq}}\right)^2 \omega^{3/2}\right] \tag{1}$$

Table 1 Creep and damage constants for Mod. 9Cr-1Mo steel at 650 °C [43]

A	n	χ	q_2	B	α
1.09×10^{-20}	8.46	7.10	4.00	7.85×10^{-17}	0.19

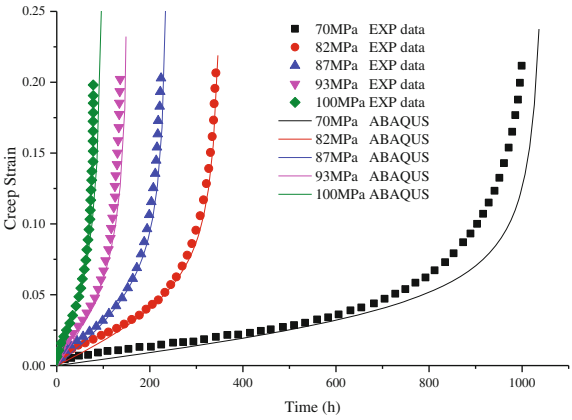

Fig. 1 Uniaxial creep validation of finite element analyses

$$\dot{\omega} = \frac{B[1-\exp(-q_2)]}{q_2}\sigma_{\mathrm{r}}^{\chi}\exp(q_2\omega) \tag{2}$$

$$\sigma_{\mathrm{r}} = \alpha\sigma_1 + (1-\alpha)\sigma_{\mathrm{eq}} \tag{3}$$

where $\dot{\varepsilon}_{ij}^{\mathrm{c}}$, σ_{eq} and S_{ij} are the multiaxial creep strain rate components, the von Mises equivalent stress, and the deviatoric stress components, respectively. The damage parameter ω represents the condition of the material deterioration in creep regime, which varies from 0 to 1 indicating virgin material and fully damaged material respectively. A, B, n, χ and q_2 are the material constants in Norton's law, which can be obtained in general by curve fitting. σ_{r} is the rupture stress.

The L-M model is implemented by the CREEP subroutine in ABAQUS, and the CREEP subroutine is verified by the uniaxial creep tests in [37]. All the constant parameters for the L-M model were listed in Table 1 [43]. Comparisons of the creep curves under different applied stresses obtained by creep tests and the present CREEP subroutine with ABAQUS are given in Fig. 1. It can be seen from Fig. 1 that the test data and the finite element analyses curves are correlated very well, which indicates that the L-M model can accurately represent the creep behavior of modified 9Cr-1Mo material and the subroutine codes are also validated.

2.2 General Hardening Elasto-plastic Constitutive Model with Damage

The calculation of structure limit load is dependent on the yield strength (YS) and ultimate tensile strength (UTS) of material. However, both of the YS and UTS of modified 9Cr-1Mo steel material are not constant under creep condition. It is revealed that YS and UTS would decrease with the increment of the temperature and creep damage increases due to material deterioration [44, 45]. Therefore, it is essential to induce creep damage into elasto-plastic constitutive model.

Ramberg-Osgood (R-O) equation [46] is an elasto-plastic constitutive model with an exponent law and widely used to describe stress-strain curve of ductile material with general hardening behavior. Hence, the R-O model has been employed in current paper for modified 9Cr-1Mo steel and the equation is given as

$$\varepsilon = \varepsilon_e + \varepsilon_p = \frac{\sigma}{E} + \left(\frac{\sigma}{H_{RO}}\right)^{1/n_{RO}} \tag{4}$$

where ε, ε_e, ε_p and E are total strain, elastic strain, plastic strain and Young's module, respectively. n_{RO} and H_{RO} are material constants and given by [47] (Table 2)

$$n_{RO} = \frac{1 + 1.3495\left(\frac{\sigma_{ys}}{\sigma_{uts}}\right) - 5.3117\left(\frac{\sigma_{ys}}{\sigma_{uts}}\right)^2 + 2.9643\left(\frac{\sigma_{ys}}{\sigma_{uts}}\right)^3}{1.1249 + 11.0097\left(\frac{\sigma_{ys}}{\sigma_{uts}}\right) - 11.7464\left(\frac{\sigma_{ys}}{\sigma_{uts}}\right)^2} \tag{5}$$

$$H_{RO} = \frac{\sigma_{uts}\exp(n_{RO})}{n_{RO}^{n_{RO}}} \tag{6}$$

The modified R-O constitutive model considering the material deterioration due to the creep damage is defined as below

$$\varepsilon = \frac{\sigma}{E} + \left(\frac{\sigma}{D_{ur}H_{RO}}\right)^{1/n_{RO}} \tag{7}$$

where D_{ur} is the UTS damage ratio which is proposed by Du et al. [49,50]. Considering the creep damage, the limit analysis can be implemented via the modified R-O constitutive model and the L-M creep model at high temperature.

Table 2 Elasto-plastic properties for Mod. 9Cr-1Mo steel at 650 °C [44, 48]

E (GPa)	ν	σ_{ys} (MPa)	σ_{uts} (MPa)	n_{RO}	H_{RO} (MPa)
155	0.3	165	228	0.11	323.19

3 Finite Element Model

3.1 Cylindrical Pressure Vessel with Volume Defect

Only one eighth of the pressure vessel is modeled due to the symmetry of the structure. The geometry of the cylindrical pressure vessel with volume defect is shown schematically in Fig. 2.

In Fig. 2, R_o is the outer radius of the cylinder, R_i is the inner radius of the cylinder, T is the wall thickness of the cylinder, L is the length of cylinder, A' and B' are the half of axial and circumferential length of the volume defect, respectively, C' is the depth of the volume defect.

Define the dimensionless axial length ratio, circumferential ratio and depth ratio of the volume defect as $a = A'/B'$, $b = C'/B'$ and $c = C'/T$ respectively. The ratio of outer radius versus inner radius of cylinder is denoted by $K = R_o/R_i$. The basic geometry parameters are listed in Table 3. In order to calculate the limit load of cylindrical pressure vessel structure with different shape volume defect and creep time, the following non-dimension parameters are considered,

a assigns 1.0 or 3.0,
b assigns 1/1, 1/3 or 1/4,
c assigns 0.33, 0.5 or 0.6,
t creep time (hours), whose values are ranging from 0 to 10000.

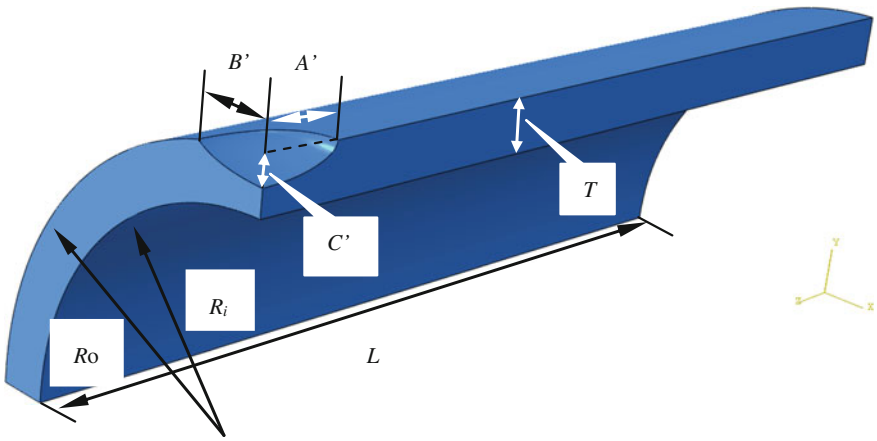

Fig. 2 Dimensions of the cylindrical pressure vessel with volume defect

Table 3 The basic geometry parameters of cylindrical pressure vessel structure

R_o (mm)	R_i (mm)	L (mm)	T (mm)	K
550	460	1500	90	1.20

3.2 Piping with Local Wall-Thinning

A quarter model of the piping with wall-thinning is modeled due to the symmetry of the structure. The geometry of the piping with local wall-thinning is shown schematically in Fig. 3.

Where R_o is the outer radius of piping, R_i is the inner radius of pipe, T is the wall thickness of pipe, L is the length of pipe, A' and B' are the half of axial and circumferential length of the local wall-thinning respectively, and C' is the depth of the local wall-thinning. The fillet is created along the corner of local wall-thinning in order to reduce the stress concentration.

The dimensionless axial length ratio, circumferential ratio and depth ratio of the local wall-thinning are defined as $a = A'/\sqrt{R_o T}$, $b = B'/\pi R_o$ and $c = C'/T$, respectively, and the ratio of outer radius versus inner radius of pipe is defined as $K = R_o/R_i$. The basic geometry parameters are listed in Table 3. In order to calculate the limit loads of piping with different life fraction and types of local wall-thinning which include small area pit, axial pit, circumferential pit and large area pit, the following non-dimensional parameters are considered,

a, dimensionless axial length ratio of the local wall-thinning, with values 0.61, 1.0 and 3.0, respectively.

b, dimensionless circumferential length ratio of the local wall-thinning, with values 0.08 and 0.25, respectively.

c, dimensionless depth ratio of the local wall-thinning, with values 0.1, 0.3 and 0.5, respectively.

$t_{lf} = t/t_r$, life fraction, with values 0, 0.2, 0.4, 0.6 and 0.8, respectively.

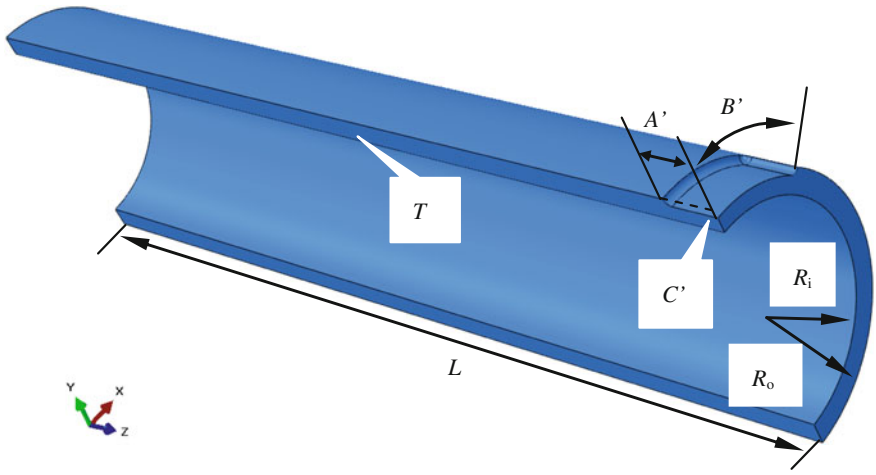

Fig. 3 Dimensions of the piping with local wall-thinning

3.3 Boundary Conditions and Applied Loading

The boundary conditions and applied loading of the cylindrical pressure vessel structure are shown in Fig. 4.

The symmetric boundary conditions (Sym-BC) are applied on the symmetry surface. P is the internal pressure which is 9.8 MPa at initial step. σ_t denotes the axial force.

The multi-loading systems in piping are more complex than that in cylindrical pressure vessel, which includes not only the internal pressure but also the bending moment M. In order to simulate the bending moment in the pipe FE model, the coupling technique is used to couple all the nodal freedoms of the end surface to a reference point (RP), and the ending moment has been applied to this RP in YOZ plane. The internal pressure is 4.81 MPa at initial step. σ_t denotes the axial force in order to simulate the closed-end condition. The symmetric boundary conditions (Sym-BC) are applied on the symmetry surface. And all the multi-loading systems and boundary conditions of the pipe structure are shown in Fig. 5.

In order to analyze effects of the combination of pressure and moment to the limit load, the limit pressure ratio, limit moment ratio and load combination ratio are defined as

$$\overline{P_L} = \frac{P_L}{P_{L0}} \tag{8}$$

$$\overline{M_L} = \frac{M_L}{M_{L0}} \tag{9}$$

$$m = \frac{\overline{M_L}}{\overline{P_L}} \tag{10}$$

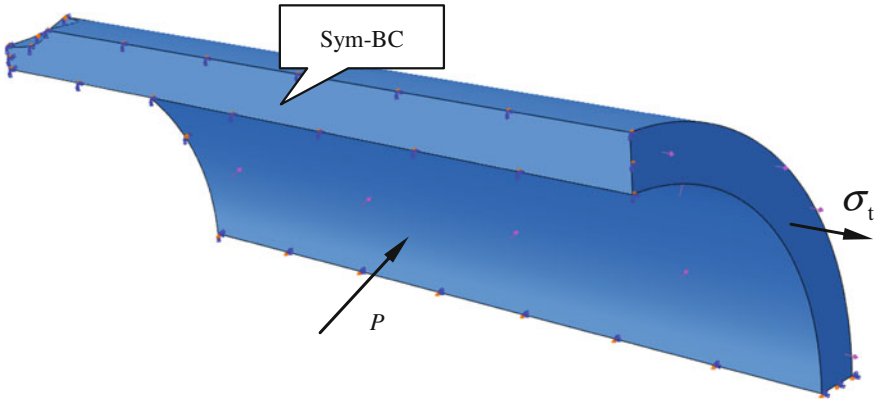

Fig. 4 Boundary conditions and applied loading of the pressure vessel structure

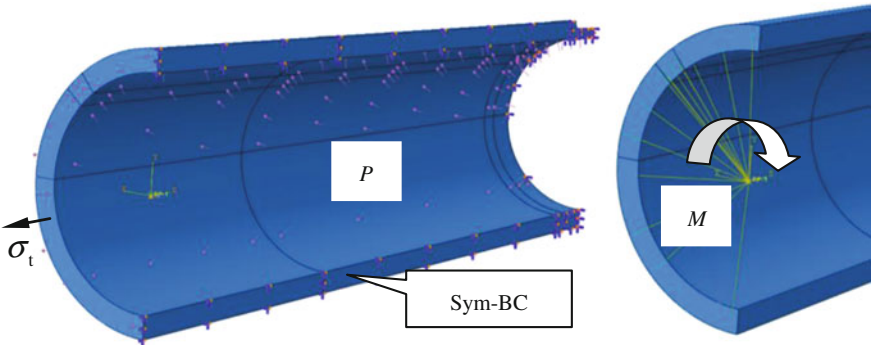

Fig. 5 Multi-loading systems and boundary condition of the pipe structure

where $\overline{P_L}$ and $\overline{M_L}$ are the limit pressure ratio and limit moment ratio, respectively. P_L and M_L are current limit pressure and current limit moment of structure with defect after service for a certain period, respectively. P_{L0} is the limit pressure of the perfect structure when the bending moment is zero and M_{L0} is the limit moment of the perfect structure when the pressure is zero. m denotes the load combination ratio, with 0, 0.5, 1.0, 2.0 and ∞, respectively. Specially, the single internal pressure condition or the single bending moment condition for piping has been accomplished when m is setting 0 or ∞.

The dimensionless defect factor considering multiple the defect dimensional parameters is defined as [51]

$$G_0 = \frac{C'}{T} \cdot \frac{A'}{B'} \cdot \frac{B'}{R_m} \cdot \sqrt{\frac{R_m}{T}} = \frac{C'A'}{T\sqrt{R_m T}} \tag{11}$$

where G_0 is dimensionless defect factor and R_m is middle radius of the cylindrical pressure vessel.

4 Numerical Results

4.1 Creep Damage and Material Deterioration

When the pressure vessels and piping with different defects have served for a long time, the field dependent R-O properties and creep damage factor fields for the pressure vessels and piping are shown in Figs. 6 and 7, where $t = t_{0.9}$ represents the service time when the creep damage is approaching to 0.9.

The results in Figs. 6 and 7 show that the von Mises stress around the local wall-thinning zone is lower than those in the other zones when the creep time is

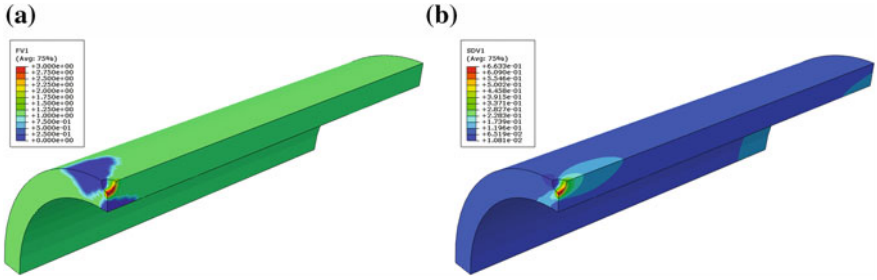

Fig. 6 Results for pressure vessel. **a** Field dependent R-O properties. **b** Current creep damage field

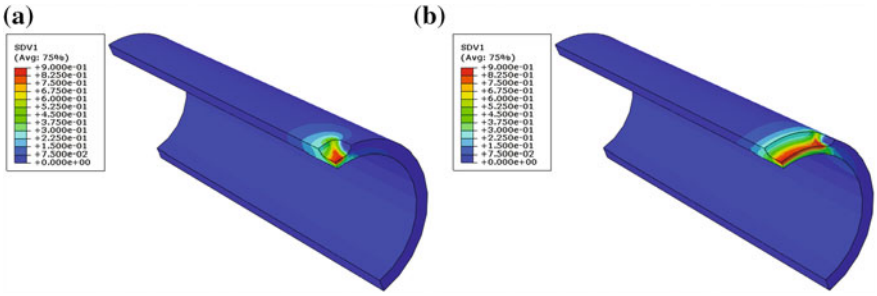

Fig. 7 The creep damage factor fields for piping with different local wall-thinning. **a** Small area pit. **b** Circumferential pit

approaching to $t_{0.9}$. It is also noted that the larger the damage factor becomes, the lower the von Mises stress is, which indicates that the effect of material deterioration can be successfully characterized by modified R-O model.

4.2 Limit State and Plastic Failure Modes for Pressure Vessel with Volume Defect

Considering the material deterioration at high temperature, the limit load and the plastic failure mode of the pressure vessel with volume defect under the creep damage condition depend on the defect ratio a, b, c and the creep time t. Assuming the radius ratio K is constant, the limit state of cylindrical pressure vessel with volume defect parameter ratios which are $a = 1.0$, $b = 1/1$ and $c = 0.33$ when creep time is ranging from 0 to 5000 h at 650 °C are shown in Figs. 8 and 9.

The results in Figs. 8 and 9 show that the modified field dependent R-O material properties are updated via USDFLD subroutine, corresponding to the current creep damage accumulated via CREEP subroutine. The maximum creep damage of cylindrical pressure vessel is increased from 0 to 0.663 and the limit load is

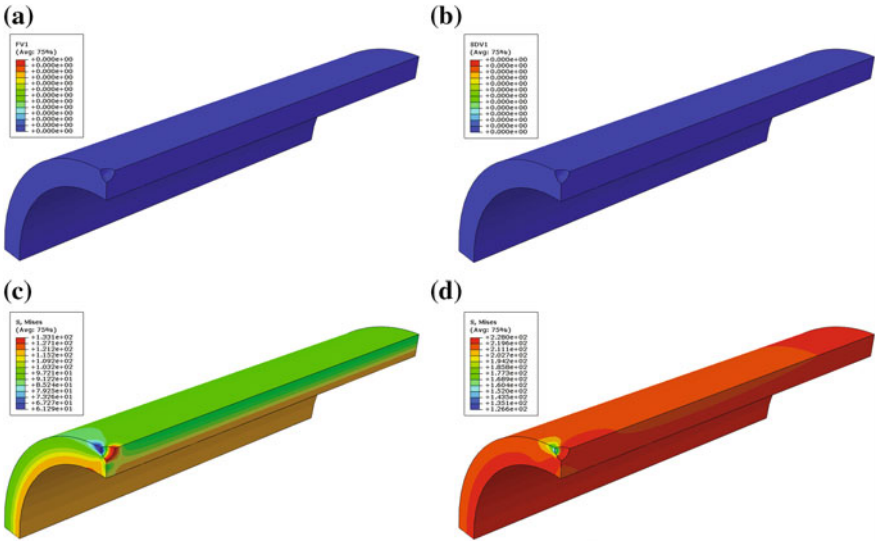

Fig. 8 The extension of plastic zone of cylindrical pressure vessel with outside volume defect ($K = 1.20$, $a = 1.0$, $b = 1/1$, $c = 0.33$, $t = 0$ h). **a** Field dependent R-O properties. **b** Current creep damage field. **c** von Mises stress field under $P = 22.12$ MPa. **d** Limit load state ($P = 42.64$ MPa)

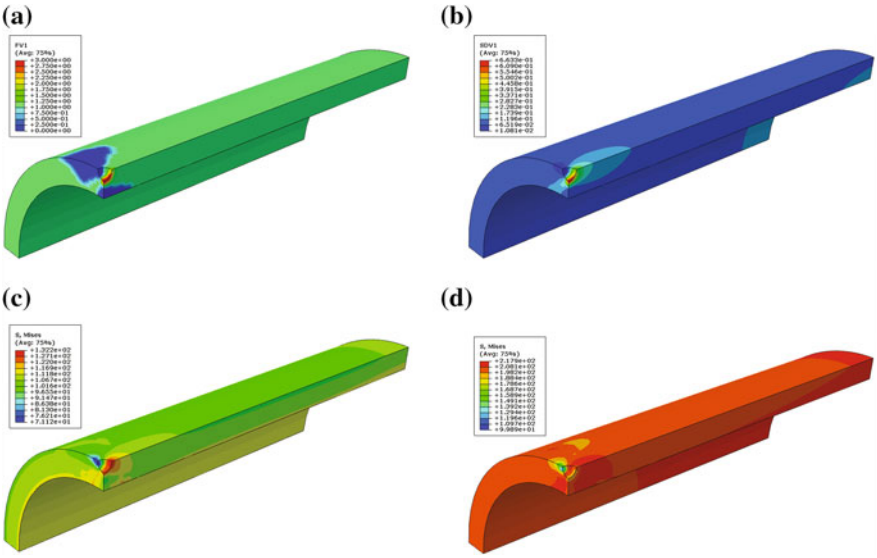

Fig. 9 The extension of plastic zone of cylindrical pressure vessel with outside volume defect ($K = 1.20$, $a = 1.0$, $b = 1/1$, $c = 0.33$, $t = 5000$ h). **a** Field dependent R-O properties. **b** Current creep damage field. **c** von Mises stress field under $P = 22.12$ MPa. **d** Limit load state ($P = 38.76$ MPa)

decreased from 42.64 to 38.76 MPa. Under the limit load state, the von Mises equivalent stresses around the high damage zone are less than those in the same places when creep time is 0, which means that the material strengths around the defect are reduced with accumulation of the damage. It can be indicated that the modified R-O damage model associated with the L-M creep damage model is implemented successfully though ABAQUS via subroutines. The initial plastic zone locates at the bottom of spherical pit when the defect ratios are small ($a = 1.0$, $b = 1/1$, $c = 0.33$). With the increment of internal pressure, the plastic zone is expended along the axial direction until almost the whole structure turns into plastic flow state, which means that the limit state is reached, and the failure mode of pressure vessel is the global structure plastic failure.

4.3 Limit Load Ratio with Defect Ratio for Pressure Vessel

By processing the results with zero curvature method, the curves of volume defect ratios to limit load ratio of cylindrical pressure vessel structure under high temperature are shown in Fig. 10.

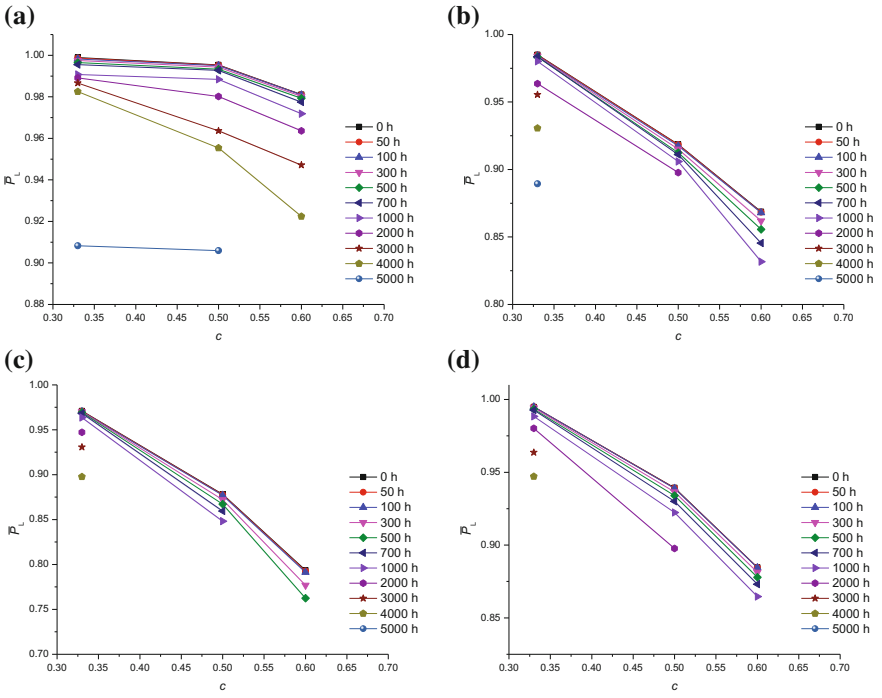

Fig. 10 Relationship of the limit load ratio with volume defect ratio. **a** $a = 1.0$, $b = 1/4$. **b** $a = 3.0$, $b = 1/1$. **c** $a = 3.0$, $b = 1/3$. **d** $a = 3.0$, $b = 1/4$

It can be seen from Fig. 10 that, with the increment of defect depth ratio c, the limit load ratio presents the descending tendency. The smaller the defect circumferential length ratio b is, the faster the limit load ratio decreases. In a similar way, the larger the defect axial length ratio a is, the faster the limit load ratio decreases. With the high creep damage rate, the secondary and tertiary creep stages are shorten substantially, and the limit load ratio decreases rapidly, even the limit load could not exist when the high creep damage zone appeared in a number of elements along the thickness of the cylindrical pressure vessel. Therefore, the defect ratio must be restricted carefully to ensure the safety of the pressure vessel structure at high temperature.

4.4 *Plastic Failure Modes at Limit States When Piping Under Multi-loading Condition*

The limit load and the von Mises stress results with different type of local wall-thinning (small area pit, circumferential pit, axial pit and large area pit) are given in Fig. 11.

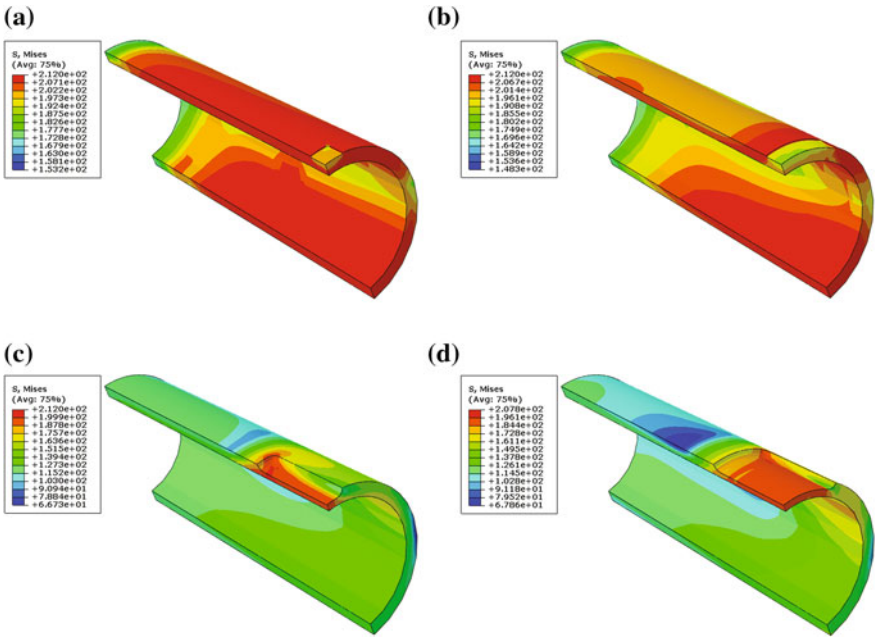

Fig. 11 The limit states of piping after serving for $t_{0.9}$ hours with different local wall-thinning and small defect depth under both internal pressure and bending moment loading condition. **a** Small area pit. **b** Circumferential pit. **c** Axial pit. **d** Large area pit

The failure modes of piping with local wall-thinning defect at limit states can be found from Fig. 11 when both the internal pressure and bending moment are applied. When both of the load combination ratio and the depth ratio are relatively small, which means the internal pressure is predominant compared with the bending moment, almost all the zones of the piping are getting into plastic flow state if the type of local wall-thinning is small area pit or circumferential pit. It means that the limit state of piping is reached, and the failure mode of piping is global plastic failure. Whereas, only the defect area of piping is getting into plastic flow state if the local wall-thinning type is axial pit or large area pit, and the plastic hinge is emerged in pit. It can be indicated that the failure modes of these types of piping are

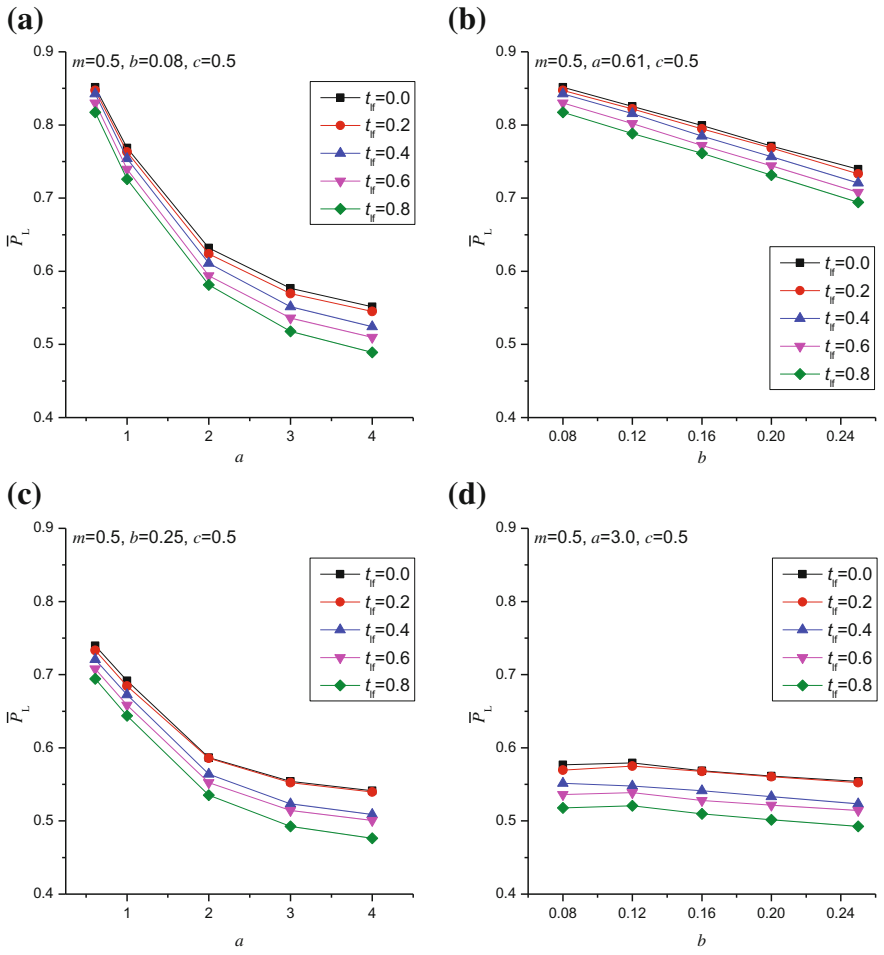

Fig. 12 Limit loads versus the ratios of local wall-thinning The limit states of piping after serving for $t_{0.9}$ hours with different local wall-thinning and small defect depth under both internal pressure and bending moment loading condition. **a** $m = 0.5, b = 0.08, c = 0.5$. **b** $m = 0.5, a = 0.61, c = 0.5$. **c** $m = 0.5, b = 0.25, c = 0.5$. **d** $m = 0.5, a = 3.0, c = 0.5$

local plastic failure. However, if the defect depth ratio is relative large, the failure modes of piping are changed to the local plastic failure if the local wall-thinning type is small area pit or circumferential pit. The failure modes of the other type of defect are the same as the small defect depth ratio.

4.5 Limit Load Ratio with Defect Ratio for Piping

Using the numerical method for the limit load of piping under elevated temperature proposed previously, the limit loads are calculated at each service timeline, then the limit pressure ratios $\overline{P_L}$ and the limit moment ratios $\overline{M_L}$ are obtained for the piping with one local wall-thinning defect type. By changing the defect ratios, all the limit loads for piping with local wall-thinning defect can be completed. Figure 12 shows the effect of defect ratios on the limit loads.

In order to analyze the effect of defect ratios a and b on the limit loads, the depth ratio c is set as a constant parameter ($c = 0.5$). It can be seen from Fig. 12 that, when the load combination ratio is relatively small, all the limit pressure ratios decrease with the increment of the service time due to the material deterioration, meanwhile, the limit pressure ratios also decrease sharply with the increment of axial length ratio a and circumferential ratio b. However, ratio b can be ignored when ratio a is large enough ($a = 3.0$), which indicates that the axial length ratio has main influence on the limit load when the internal pressure loading is dominant.

5 Conclusion

In this research, numerical limit analysis of modified 9Cr-1Mo steel pressure vessels with volume defect and piping with local wall-thinning at 650 °C has been studied. The creep behavior with L-M damage model and general hardening behavior with modified R-O model have been implemented in ABAQUS with the CREEP and USDFLD subroutine. The limit load under elevated temperature is defined as the load-carrying capacity after the structure serviced for a long time. The UTS damage ratio has been defined to consider the creep damage, and then, the R-O model has been modified by embedding the UTS damage ratio to take into account material deterioration. Thus, a numerical solution method for the limit load at elevated temperature considering creep damage due to material deterioration has been proposed.

Meanwhile, examples for pressure vessels and piping with different sizes of defects and multi-loading systems have been calculated and analyzed, and the following conclusions can be drawn:

1. The service life and limit load of pressure vessels and piping are very sensitive to the defect ratio at high temperature. The failure mode of pressure vessels and

piping is global structure plastic failure when the defect ratio is relative small, whereas the failure mode is local plastic failure in the limit state when defect ratio is relative large.

2. Large defect can speed up the accumulation of creep damage during creep deformation. With the high creep damage rate, the secondary and tertiary creep stages have been shorten substantially, and the limit load ratio is reduced rapidly, even the limit load is no longer exist when the creep damage zone is achieved in a number of elements along the thickness of the cylindrical pressure vessel. Therefore, the defect ratio must be restricted carefully to ensure the safety of pressure vessels and piping at high temperature.
3. For the piping with local wall-thinning at high temperature, the axial length ratio a has main influence on the limit load when the load combination ratio $m \leq 0.5$, which indicates that the internal pressure is dominant. In a similar way, the limit load is mainly effected by the circumferential ratio b when the load combination ratio $m \geq 2.0$, which indicates that the bending moment is dominant. If the load combination ratio $0.5 < m < 2.0$, the limit loads are not dependent on the single defect ratio.

Acknowledgements This work was supported by the National Science Foundation for Distinguished Young Scholars of China (Project No. 11325211) and National Natural Science Foundation of China (Project No. 11302023).

References

1. Perrin IJ, Hayhurst DR (1996) Creep constitutive equations for a 0.5Cr-0.5Mo-0.25V ferritic steel in the temperature range 600–675 °C. J Strain Anal Eng Des 31:299–314
2. Drucker DC (1951) A more fundamental approach to plastic stress-strain relations. J Appl Mech-T ASME 18(3):487–491
3. Hill R (1950) The mathematical theory of plasticity. The Oxford engineering science series. Clarendon Press, Oxford
4. Hodge PG (1963) Limit analysis of rotationally symmetric plates and shells. Prentice-Hall series in solid and structural mechanics, vol 147. Prentice-Hall, Englewood Cliffs, N. J.
5. Hodge PG Jr (1970) Limit analysis with multiple load parameters. Int J Solids Struct 6(5): 661–675
6. Belytschko T, Hodge PG (1970) Plane stress limit analysis by finite elements. J Eng Mech Div 96(6):931–944
7. Maier G, Munro J (1982) Mathematical programming applications to engineering plastic analysis. Appl Mech Rev 35(12):1631–1643
8. Chen HF (1998) Numerical methods for limit analysis and reference stress determination of structures under multi-loading systems and their engineering applications. Tsinghua University, Beijing (in Chinese)
9. Han LH, He SY, Wang YP, Liu CD (1999) Limit moment of local wall thinning in pipe under bending. Int J Press Vessels Pip 76(8):539–542
10. Kim JW, Na MG, Park CY (2008) Effect of local wall thinning on the collapse behavior of pipe elbows subjected to a combined internal pressure and in-plane bending load. Nucl Eng Des 238(6):1275–1285

11. Kim YJ, Kim J, Ahn J, Hong SP, Park CY (2008) Effects of local wall thinning on plastic limit loads of elbows using geometrically linear FE limit analyses. Eng Fract Mech 75(8): 2225–2245
12. Mackenzie D, Shi J, Boyle JT (1994) Finite-element modeling for limit analysis by the elastic compensation method. Comput Struct 51(4):403–410. doi:10.1016/0045-7949(94)90325-5
13. Liu YH, Cen ZZ, Xu BY (1995) Numerical limit analysis of cylindrical-shells with part-through slots. Int J Press Vessels Pip 64(1):73–82
14. Liu YH, Cen ZZ, Xu BY (1995) Numerical investigation of limit loads for the pressure vessels with part-through slots. Acta Mech Solida Sin 8(3):263–276
15. Liu YH, Cen ZZ, Xu BY (1995) A numerical-method for plastic limit analysis of 3-D structures. Int J Solids Struct 32(12):1645–1658
16. Liu YH, Zhang XF, Cen ZZ (2004) Numerical determination of limit loads for three-dimensional structures using boundary element method. Eur J Mech A-Solid 23(1): 127–138
17. Liu YH, Zhang XF, Cen ZZ (2005) Lower bound shakedown analysis by the symmetric Galerkin boundary element method. Int J Plast 21(1):21–42
18. Du XH, Liu DH, Liu YH (2015) Numerical limit load analysis of 3D pressure vessel with volume defect considering creep damage behavior. Math Probl Eng 1–13
19. Arzt E, Wilkinson DS (1986) Threshold stresses for dislocation climb over hard particles—the effect of an attractive interaction. Acta Metall Mater 34(10):1893–1898
20. Fournier B, Sauzay M, Pineau A (2011) Micromechanical model of the high temperature cyclic behavior of 9–12%Cr martensitic steels. Int J Plast 27(11):1803–1816
21. Böck N, Kager F (2005) Finite element simulation of the creep behaviour of 9% chromium steels based on micromechanical considerations. Paper presented at the materials science and technology 2005 conference and exhibition, Pittsburgh, PA, USA, 25–28 Sept 2005
22. Sklenička V, Kuchařová K, Dlouh SA, Krejci J (1994) Creep behaviour and microstructure of a 9%Cr steel. Paper presented at the proceedings of the conference on materials for advanced power engineering, Dordrecht, Netherlands
23. Graham A, Walles KFA (1955) Relations between long and short time properties of commercial alloys. J Iron Steel Inst 193:105
24. McVetty G (1933) Factors affecting the choice of working stresses for high temperature service. Trans ASME 55:99
25. Conway JB, Mullikin MJ (1962) An evaluation of various first stage creep equations. Paper presented at the proceedings of AIME conference, Detroit, Michigan
26. Norton FN (1929) The creep of steel at high temperature. McGraw-Hill, New York
27. Kachanov LM (1958) On destruction in creeping of materials. Izvestia Akademii Nauk SSSR, Otdelenie Tekhnicheskich Nauk 8:26–31
28. Rabotnov YN (1969) Creep problems in structural members. North-Holland series in applied mathematics and mechanics, vol 7. North-Holland Publishing Company, Amsterdam, London
29. Liu DH, Li HS, Liu YH (2015) Numerical simulation of creep damage and life prediction of superalloy turbine blade. Math Probl Eng 1–10
30. Saanouni K, Chaboche JL, Bathias C (1986) On the creep crack growth prediction by a local approach. Eng Fract Mech 25(5–6):677–691
31. Benallal A, Billardon R, Lemaitre J (1991) Continuum damage mechanics and local approach to fracture: numerical procedures. Comput Methods Appl Mech Eng 92(2):141–155
32. Hall FR, Hayhurst DR, Brown PR (1996) Prediction of plane-strain creep-crack growth using continuum damage mechanics. Int J Damage Mech 5(4):353–383
33. Hayhurst DR (2005) CDM mechanisms-based modelling of tertiary creep: ability to predict the life of engineering components. Arch Mech 57(2–3):103–132
34. Liu Y, Murakami S (1998) Damage localization of conventional creep damage models and proposition of a new model for creep damage analysis. JSME Int J Ser A: Solid Mech Mater Eng 41(1):57–65
35. Murakami S, Liu Y, Mizuno M (2000) Computational methods for creep fracture analysis by damage mechanics. Comput Methods Appl Mech Eng 183(1–2):15–33

36. McLean M, Dyson BF (2000) Modeling the effects of damage and microstructural evolution on the creep behavior of engineering alloys. J Eng Mater Technol Trans ASME 122(3): 273–278
37. Hyde TH, Becker AA, Sun W, Williams JA (2006) Finite-element creep damage analyses of P91 pipes. Int J Press Vessels Pip 83(11–12):853–863
38. Cocks ACF, Ashby MF (1980) Intergranular fracture during power-law creep under multiaxial stresses. Metal Sci 14(8–9):395–402
39. Basirat M, Shrestha T, Potirniche GP, Charit I, Rink K (2012) A study of the creep behavior of modified 9Cr-1Mo steel using continuum-damage modeling. Int J Plast 37(0):95–107
40. Xue JL, Zhou C, Wang B, Peng J (2013) Stress-strain constitutive relation of P91 steel based on creep damage. J Nanjing Univ Technol (Natural Science Edition) 35(4):33–37 (in Chinese)
41. Wang N, Liu H-Q, Tu S-T (2014) Elasto-plastic constitutive model of 2.25Cr1Mo steel considering initial creep damage. Press Vessel Technol 31(1):1–14 (in Chinese)
42. Goyal S, Laha K, Das CR, Panneerselvi S, Mathew MD (2013) Finite element analysis of effect of triaxial state of stress on creep cavitation and rupture behaviour of 2.25Cr–1Mo steel. Int J Mech Sci 75:233–243
43. Rouse JP, Sun W, Hyde TH, Morris A (2013) Comparative assessment of several creep damage models for use in life prediction. Int J Press Vessels Pip 108–109(0):81–87
44. ASME (2010) Boiler & Pressure Vessel Code Division 1. Subsection NH III. ASME, USA
45. Masuyama F (2006) Creep degradation in welds of Mod. 9Cr-1Mo steel. Int J Press Vessels Pip 83(11–12):819–825
46. Ramberg W, Osgood WR (1943) Description of stress-strain curves by three parameters. Technical Note No. 902. National Advisory Committee For Aeronautics, Washington DC
47. ASME (2010) Fitness-For-Service. API 579-1. ASME, USA
48. Takahashi Y (2008) Study on creep-fatigue evaluation procedures for high-chromium steels—part I: test results and life prediction based on measured stress relaxation. Int J Press Vessels Pip 85(6):406–422. doi:10.1016/j.ijpvp.2007.11.008
49. Du XH, Zhang J, Peng H, Liu YH (2017) Plastic limit analysis of modified 9Cr-1Mo steel pressure vessel containing volume defect with creep damage law. Int J Appl Mech 9(2): 1750025(1–29)
50 Du XH, Zhang J, Liu YH (2017) Plastic failure analysis of defective pipes with creep damage under multi-loading systems. Int J Mech Sci 128–129:428–444
51 Chen G, Liu YH (2006) Numerical theories and engineering methods for structural limit and shakedown analyses. Science Press, Beijing (in Chinese)